Anion Receptors Hot Paper

Deutsche Ausgabe: DOI: 10.1002/ange.201608384
Internationale Ausgabe: DOI: 10.1002/anie.201608384

Octulene: A Hyperbolic Molecular Belt that Binds Chloride Anions

Marcin A. Majewski, Yongseok Hong, Tadeusz Lis, Janusz Gregoliński, Piotr J. Chmielewski, Joanna Cybińska, Dongho Kim, and Marcin Stępień**

Dedicated to Jonathan L. Sessler

Abstract: *Octulene, the higher homologue of kekulene and septulene, was synthesized using the fold-in method. This new hydrocarbon macrocycle contains a large 24-membered inner circuit, which is peripherally fused to 24 benzene rings. Such an arrangement produces considerable hyperbolic distortion of the π-conjugated surface. The consequences of distortion in octulene were explored using photophysical methods, which revealed a reduced electronic band gap and greater flexibility of the π system. Octulene contains a functional cavity with a diameter larger than 5.5 Å that is capable of efficiently binding the chloride anion in a nonpolar solvent ($K_a = 2.2(4) \times 10^4\ M^{-1}$, 1% dichloromethane (DCM) in benzene). The octulene–chloride interaction is stabilized by eight weak $C(sp^2)H\cdots Cl$ bonds, providing the first example of a hydrocarbon-based anion receptor.*

In geometry, the feasibility of specific tessellations (tilings) depends on the curvature of the underlying surface.[1] The chemically relevant hexagonal tiling (Figure 1B), which provides a model of benzenoid ring fusion, fits on surfaces with constant zero Gaussian curvature ($\kappa = 0$), and notably on the Euclidean plane (as in graphene and nanographenes[2–4]) and on the cylinder (as in carbon nanotubes). Fullerenes and their fragments (buckybowls) are based on pentagonal tilings, which are compatible with the spherical curvature ($\kappa > 0$) of these structures.[5–7] Negative Gaussian curvature, much less common among aromatic molecules, can be built around seven-[8–12] or eight-membered[13–15] rings. Such systems can be called "hyperbolic nanographenes" because the pertinent ring fusion patterns can be found in hyperbolic tessellations. For instance, the classic hyperbolic system, saddle-shaped [7]circulene (**1**, Figure 1A),[8] may be viewed as a fragment of so-called truncated order-7 triangular tiling (t{3,7}, Figure 1C).

Kekulene **2**,[16] the first coronoid hydrocarbon,[17] is the smallest macrocyclic nanographene retaining planarity, and may be envisaged as the repeat unit of periodic "graphene meshes" (for example, Figure 1D). The sub-nanometer pore of **2**, similar to those investigated in graphene sheets,[18] is of potential relevance to organic electronics[19] and gas separation.[20] Kekulene is thus an interesting object for structural elaboration, and its subunit-replaced,[21,22] expanded,[22,23] and peripherally fused[24] analogues have recently been explored. In particular, positively curved (bowl-shaped) analogues of **2** were created by replacement of selected benzene units with five-membered rings.[21,22] In principle, homologation of kekulene to enlarge its central ring should produce a

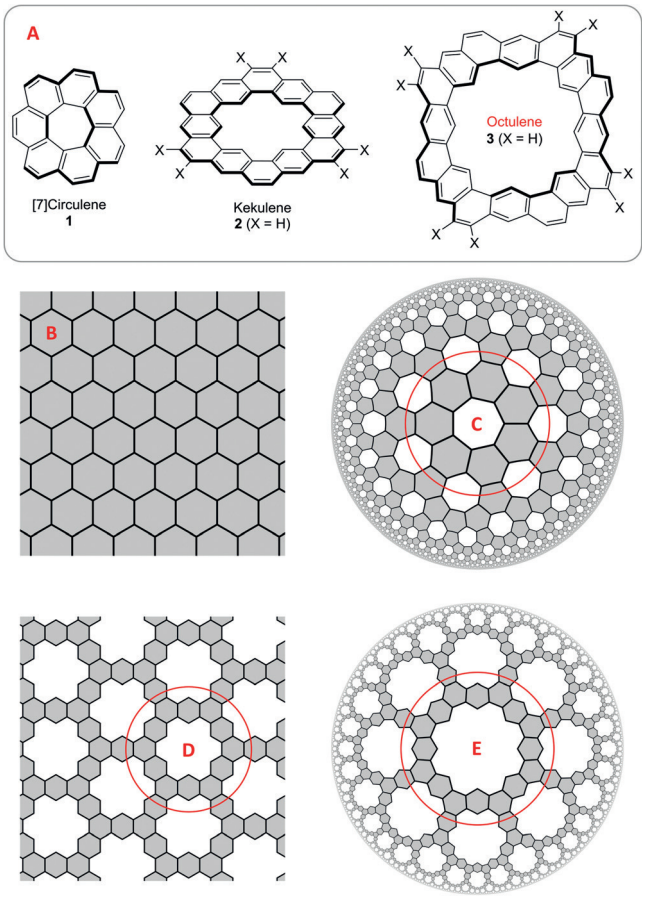

Figure 1. A) Planar and hyperbolic aromatics discussed in the introduction. B) Hexagonal tiling found in graphene. C) Molecular framework of [7]circulene embedded in the t{3,7} hyperbolic tiling. D) Planar tiling based on the kekulene ring system. E) Hyperbolic tiling based on the octulene ring system.

[*] M. A. Majewski, Prof. T. Lis, Dr. J. Gregoliński, Prof. P. J. Chmielewski, Dr. J. Cybińska, Prof. M. Stępień
Wydział Chemii, Uniwersytet Wrocławski
ul. F. Joliot-Curie 14, 50-383 Wrocław (Poland)
E-mail: marcin.stepien@chem.uni.wroc.pl
Homepage: http://www.mstepien.edu.pl
Y. Hong, Prof. D. Kim
Department of Chemistry, Yonsei University
50 Yonsei-ro, Seoul 120-749 (Korea)
E-mail: dongho@yonsei.ac.kr

Supporting information for this article can be found under: http://dx.doi.org/10.1002/anie.201608384.

hyperbolic distortion of the π system. However, in both septulene[23] and [4]chrysaorene,[22] the excess curvature is largely absorbed by valence angle deformations, leading to essentially planar molecules. Molecular modeling shows that the negative curvature should emerge in octulene (**3**, Figure 1 A), the next higher member of the kekulene–septulene series, which has an estimated internal strain of approximately 30 kcal mol^{-1}. In analogy to **1**, infinite patterns based on the octulene motif can only be constructed on a hyperbolic plane (Figure 1 E). Herein, we report the first synthesis of an octulene derivative and describe its properties; notable among these is the unexpected ability to bind chloride anions.

We attempted to synthesize octulene by using the fold-in method, which involves inner stitching of macrocyclic precursors,[7,21] and has been used with success to induce positive curvature in various bowl- and belt-like systems.[21,22,25] The McMurry cyclooligomerization of a newly designed dialdehyde building block **S4** produced a mixture of cyclic and linear products from which cyclophanes **4a** (16 %), **5a** (11 %), and **6a** (7.4 %), were isolated chromatographically (Scheme 1). **6a** was also prepared in higher yield (18 %) using the previously developed Wittig-based strategy.[22,26] The three macrocyclic precursors **4a**–**6a** were structurally characterized in solution and in the solid state, as described in the Supporting Information.

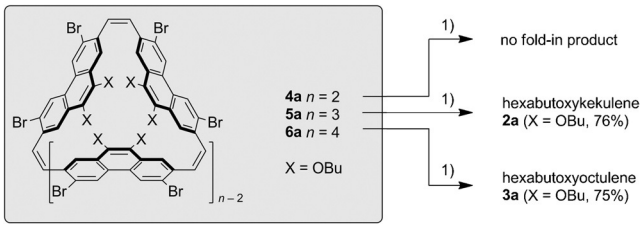

Scheme 1. The fold-in synthesis of substituted kekulene and octulene from the corresponding phenanthrenophanes. For clarity, the generalized structures for **4a**–**6a** are drawn in an all-*syn* conformation. Reagents and conditions, 1): Ni(1,5-cyclooctadiene)$_2$, 2,2′-bipyridyl, *N*,*N*-dimethylformamide, 100 °C.

The fold-in reaction was attempted on all three cyclophanes, which were subjected to the Ni^0-mediated Yamamoto homocoupling. The expected fold-in product of **4a** ("tetrulene") was not observed to form, as might be expected from the extremely high internal strain of the target framework. In contrast, **5a** and **6a** cleanly produced the respective coronoid targets, kekulene **2a** and octulene **3a**, which were isolated chromatographically in 76 % and 75 % yield, respectively. The molecular formulae of both systems were confirmed using high-resolution mass-spectrometric analyses.

In contrast to unsubstituted kekulene and septulene, known for their extremely low solubility,[16,23] **2a** dissolves readily in many organic solvents. A ^{1}H NMR spectrum of **2a** recorded in CD_2Cl_2 is consistent with the D_{3h} symmetry of the molecule, with a diagnostic low-field resonance of the inner protons (9.90 ppm). On lowering the temperature (Supporting Information, Figure S11), the aromatic ^{1}H signals of **2a** progressively broadened and shifted to higher field. When the sample was cooled from 300 to 220 K, the inner H signal shifted from 9.90 to 9.53 ppm, with a concomitant linewidth increase from approximately 7 to 170 Hz. Below 220 K, partial decoalescence was observed, but the spectrum was insufficiently resolved to permit a more detailed analysis. The dynamic behavior of the system, and the high-field relocations of aromatic resonances, are consistent with the temperature dependent π-stacking aggregation, which is however too fast or insufficiently specific to yield a well-resolved dimer spectrum.[27] The feasibility of π-stacking was further demonstrated in a single-crystal analysis of **2a**, which revealed the formation of infinite, slipped stacks in the solid state (Figure 2 B; Supporting Information, Figure S8).The noticeable twisting of the kekulene core in the crystal of **2a** (0.20 Å mean-plane deviation) apparently serves to maximize intermolecular interactions at the center of the macrocycle.

The ^{1}H NMR spectrum of octulene **3a** is very similar to that of **2a**, confirming the homologous structures of these two ring systems. However, temperature-dependent changes of the aromatic signals are far less pronounced for octulene (Supporting Information, Figure S11). At 220 K, the inner H signal is relocated by only −0.02 ppm relative to its position at 300 K (10.10 ppm), with only a small increase in linewidth (2.5 to 6.5 Hz). This observation implies considerable suppression of π-stacking in solution, in comparison with **2a**, which is in agreement with the presumed non-planar geometry of the octulene core.

According to DFT calculations, unsubstituted **3** takes the shape of a very deep saddle with a vertical extent of 9.2 Å (Figure 2 C,D), and its geometry is insignificantly affected by substitution with methoxy groups (**3b**, X = OMe; Supporting Information). The formal eight-fold symmetry of **3**, which could be realized on a hyperbolic plane, is not attainable in chemical reality. Because of the saddle distortion, the highest possible point symmetry of **3** and **3a**,**b** is D_{2d}, which should lead to diastereotopic differentiation of CH_2 signals in the ^{1}H NMR spectrum of the butyl-substituted **3a**. The absence of diastereotopicity in the experimental spectrum may result from accidental isochrony of the corresponding methylene protons, but it can also be caused by a rapid "roller coaster" motion of the macrocycle, which would lead to dynamic averaging of the diastereotopic CH_2 pair. In unsubstituted **3**, such a roller coaster shift is predicted to occur with ease, with an estimated energy barrier of less than 1 kcal mol^{-1} (Supporting Information, Figure S18).

Steady-state absorption spectra of **2a** and **3a** are characteristic of highly symmetrical cyclic aromatics, with near forbidden lowest energy transitions (Figure 3). However, the vibronic pattern of the main absorption is less clearly resolved in **3a**, suggesting a greater flexibility of the distorted octulene ring. In line with this assumption, **3a** yields a sharper and more intense absorption at low temperatures (77 K in 2-methyltetrahydrofuran; Supporting Information, Figure S13). The effects of flexibility can also be inferred from the fluorescence behavior of **3a**. In comparison with **2a**, octulene exhibits a lower fluorescence quantum yield (3.6 % vs. 5.2 %), and a less clear vibronic structure in the emission band. Accordingly, fluorescence decay times of 20.2 and 15.0 ns were measured for **2a** and **3a**, respectively, by means

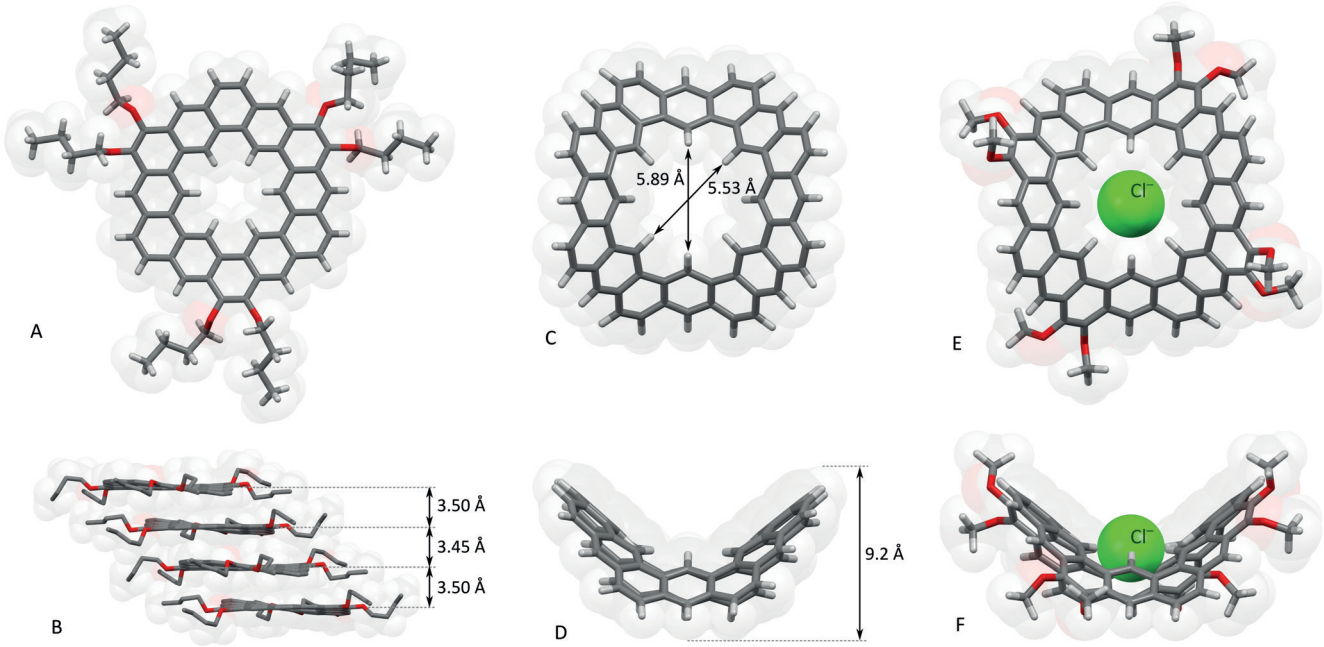

Figure 2. A) Molecular structure of **2a** determined in an X-ray crystallographic analysis. B) π-Stacked columns observed in the crystal structure of **2a**. C,D) Gas-phase DFT geometry of the unsubstituted octulene **3**. E,F) Gas-phase DFT geometry of the chloride adduct **3b**·Cl^- (level of theory: ωB97XD/6-31G(d,p)).

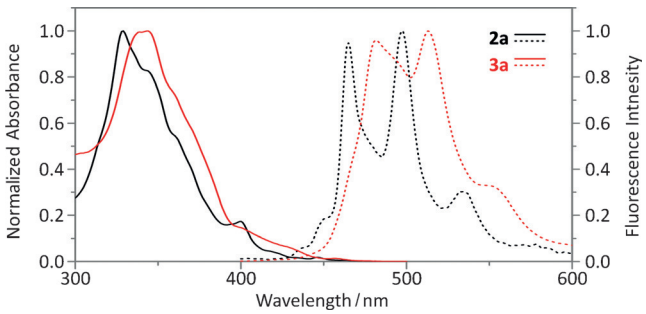

Figure 3. Normalized absorption and emission spectra of **2a** and **3a** (toluene, 300 K).

of time-correlated single-photon counting (TCSPC). While the radiative rates determined for **2a** and **3a** were similar (Supporting Information, Table S1), the observed difference in non-radiative rates (4.7 vs. $6.4\times10^7\ s^{-1}$ for **2a** and **3a**, respectively) indicates that a more efficient non-radiative channel is available for octulene, which may be tentatively linked to the dynamic distortion of the chromophore. No fast decay processes associated with vibrational dynamics were observed in femtosecond-transient absorption measurements (Supporting Information, Figure S15).

Femtosecond transient absorption anisotropy measurements performed for **2a** and **3a** (fs-TAA; Supporting Information, Figure S16) showed that, following an ultrafast initial depolarization (<200 fs), the anisotropy was static over the first 8 ps after excitation, with r_0 values of 0.07 and 0.06 for **2a** and **3a**, respectively. The subsequent decay was monoexponential for both systems and was slower for octulene ($\tau_r = 500$ ps for **3a** vs. 350 ps for **2a**). Both r_0 values are within the limit expected for disk-like molecules ($r_0 < 0.1$),[28] for which dephasing occurs between pairs of degenerate, orthogonally polarized states. The smaller r_0 value observed for **3a** likely originates from structural distortions of the octulene core. TCSPC fluorescence anisotropy data obtained for **3a** and **2a** indicate similar rotational diffusion rates ($\tau_r = 510$ ps and 350 ps, respectively; Supporting Information, Figure S17).

Magnetic and structural aromaticity indices (Supporting Information, Figures S19–S21) confirm the benzenoid character of π conjugation in **3**. Specifically, they provide evidence for the preferential localization of Clar sextets in the linearly fused benzene rings, previously observed in kekulene and septulene. The red shifts in the absorption and emission spectra indicate a reduction of the electronic band gap of **3a** relative to that of **2a** (Figure 3). Such a change is confirmed by electrochemistry data and TD-DFT calculations (Supporting Information). The decrease of Kohn–Sham band gaps (3.56, 3.43, and 3.23 eV for **2**, septulene, and **3**, respectively), caused principally by the destabilization of the HOMO, is faster than might be expected in a series of homologous π systems (typically obeying the $1/n$ relationship[29]). The smaller than expected band gap of **3** may indicate a contributing influence of the hyperbolic distortion, similar to the effect observed in distorted porphyrin chromophores for example.[30]

The large cavity of octulene is surrounded by eight $C(sp^2)$–H bonds pointing approximately towards its center, and we envisioned that it might act as a receptor for small guests. Neutral anion receptors based on CH donors[31] are inherently weakly coordinating, and they typically contain highly polarized subunits (for example, CF bonds,[32] acetals,[33] triazoles,[34] or cyanostilbenes[35]) that enhance

anion binding. In comparison with the triazole-based receptor described by Li and Flood (**LF**),[34] octulene features much lower electrostatic potential (ESP) on the inner hydrogens (Table 1). Nevertheless, the central cavity has similar dimensions in the two systems, and the completely fused octulene macrocycle was expected to provide a more rigid binding environment.

Table 1: Binding data for octulene.

Parameter	**3**	**3a**/**3b**[a]	**LF**
H···H diameter [Å][b]	5.53–5.89	5.55–5.89	5.54–5.84
ESP [kcal/mol][b,c]	24	23	41-55
Cl binding energy[b,d]	−34.9	−34.5	−60.3
H···H with bound Cl^- [Å][b]	5.43–5.62	5.43–5.61	5.22–5.91
Distortion energy[b]	1.55	1.98	2.38
K_a (Cl^-) [M^{-1}][e]		$2.2(4)\times10^4$[f]	$1.3(3)\times10^5$[g]
DCM binding energy[b,d]	−9.46	−9.45	−10.45

[a] Binding constants for **3a**, other data for **3b**. [b] ωB97XD/6-31G(d,p) in vacuo; [c] electrostatic potential on inner hydrogen atoms (0.002 a.u. density isosurface). [d] Counterpoise-corrected. [e] Binding constants for Cl^-. [f] 1% CD_2Cl_2 in C_6D_6, 280 K. [g] CH_2Cl_2, 298 K, as in ref. [34].

Initial anion binding experiments, monitored using ^{1}H NMR spectroscopy, showed downfield relocations of the inner CH signal when solutions of octulene **3a** in CD_2Cl_2 were treated with a large excess of tetrabutylammonium salts (TBAX; X = F, Cl, Br, I, CN). Reference experiments performed for kekulene **2a** showed no effect, indicating that the change seen for **3a** may indeed reflect anion binding in the cavity. This hypothesis was further supported by the anion dependence of the effect observed for octulene. The strongest interaction was observed with the chloride anion, which was therefore selected for subsequent study. Remarkably, it was found that the binding was significantly enhanced in benzene solutions. A titration performed in C_6D_6, containing 1% CD_2Cl_2 to solubilize TBACl, showed separate resonances for inner protons of **3a** and **3a**·Cl^- (10.20 and 12.10 ppm, respectively; Figure 4), indicative of slow anion exchange. The large high-field shift observed for the **3a**·Cl^- complex is a characteristic feature of the bound state of CH-based anion receptors.[34] Because of smaller absolute shift differences, the outer protons yielded dynamically averaged signals. Fitting the chloride-induced shift changes with the 1:1 binding model yielded an association constant $K_a = 2.4(2)\times10^4\,M^{-1}$. The proposed binding stoichiometry was verified by a ^{1}H NMR continuous variation (Job) experiment.

Deviations of the binding isotherms from the 1:1 model may be attributed to the formation of a tight ion pair with the TBA cation, with a stoichiometry [**3a**·Cl^-][TBA^+], which is expected to be stabilized in a nonpolar solvent medium.[36] The formation of such an ion pair can be inferred from the high-field relocations of TBA signals (ca. −0.6 ppm relative to free TBACl), observed at low TBACl:**3a** molar ratios. Such a shift is consistent with the location of TBA^+ in the deshielding zone of the octulene ring system, that is, above or below the aromatic surface. In the course of the titration, the TBA shifts increased gradually, indicating rapid exchange between the octulene-bound ion pair and the bulk TBA cation. The binding equilibria can be further complicated by the formation of higher aggregates of TBACl, analogous to those observed in chloroform.[37] Such assemblies are likely to persist in benzene solution and may even be involved in binding to octulene at higher salt concentrations.

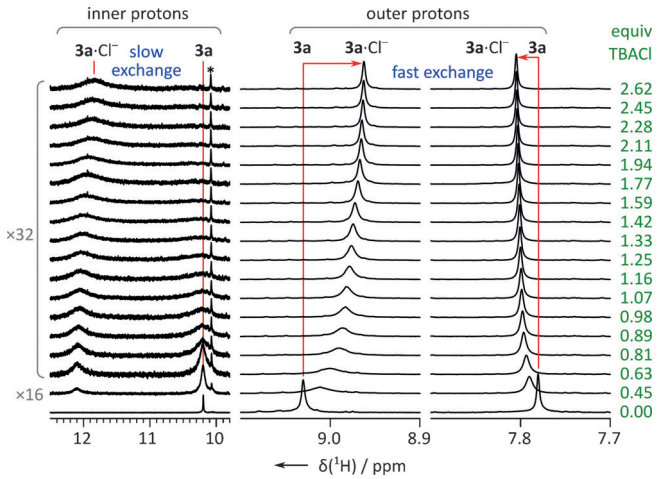

Figure 4. Changes in the ^{1}H NMR spectrum of **3a** during titration with tetrabutylammonium chloride (TBACl, 600 MHz, 280 K, 0.14 mM **3a**, 1% CD_2Cl_2 in C_6D_6).

The excellent fit of the chloride ion in the octulene cavity was confirmed by DFT calculations (Figure 2E,F, Table 1), which yielded a gas-phase binding energy of −34.5 kcal mol^{-1} for **3b**·Cl^-. The cavity is predicted to undergo a slight contraction upon anion binding, with a corresponding distortion energy of only approximately 2 kcal mol^{-1}. The apparent K_a for chloride binding determined in nearly pure benzene indicates that the preorganized cavity in **3a** can effectively compete for Cl^- with a solvent that provides a chemically similar environment for the anions (multiple $C(sp^2)H$ bonds, ESP(H) ca. 18 kcal mol^{-1}). The much weaker binding in DCM (by ca. 4 orders of magnitude) can be attributed, not only to the potentially stronger anion solvation, but also, to the ability of a DCM molecule to fill the cavity in **3a**. The binding energy calculated for **3b**·DCM (Table 1) is lower than for **3b**·Cl^- but nevertheless indicates that DCM binding may compete at bulk solvent concentrations.

Octulene, the first reported coronoid ring system with a distinct hyperbolic distortion, demonstrates the efficacy of the fold-in method in the synthesis of negatively curved aromatics. More surprisingly, octulene reveals the possibility of using hydrocarbon macrocycles as anion receptors, offering new insight into the thermodynamics of anion binding in nonpolar environments. Efforts to create further receptor molecules based on this principle are currently underway.

Acknowledgements

The project was funded by the National Science Centre of Poland (DEC-2012/07/E/ST5/00781 to M.S. and DEC-2015/19/N/ST5/00760 to M.A.M.). The research at Yonsei

University was supported by the Global Research Laboratory (GRL) Program (2013K1A1A2A02050183) of the Ministry of Education, Science and Technology (MEST) of Korea. Quantum-chemical calculations were performed in the Centers for Networking and Supercomputing of Wrocław and Poznań and at the Korea Institute of Science and Technology Information (KISTI). We thank Prof. Jay Siegel for helpful discussion.

Keywords: anion binding · aromaticity · hydrocarbons · organic synthesis · photophysics

How to cite: *Angew. Chem. Int. Ed.* **2016**, *55*, 14072–14076
Angew. Chem. **2016**, *128*, 14278–14282

[1] J. H. Conway, H. Burgiel, C. Goodman-Strauss, *The Symmetries of Things*, A. K. Peters, Wellesley, Mass, **2008**.
[2] K. K. Baldridge, J. S. Siegel, *Angew. Chem. Int. Ed.* **2013**, *52*, 5436–5438; *Angew. Chem.* **2013**, *125*, 5546–5548.
[3] A. Narita, X.-Y. Wang, X. Feng, K. Müllen, *Chem. Soc. Rev.* **2015**, *44*, 6616–6643.
[4] M. Stępień, E. Gońka, M. Żyła, N. Sprutta, *Chem. Rev.* **2016**, DOI: 10.1021/acs.chemrev.6b00076.
[5] Y.-T. Wu, J. S. Siegel, *Chem. Rev.* **2006**, *106*, 4843–4867.
[6] V. M. Tsefrikas, L. T. Scott, *Chem. Rev.* **2006**, *106*, 4868–4884.
[7] M. Stępień, *Synlett* **2013**, 1316–1321.
[8] K. Yamamoto, T. Harada, M. Nakazaki, T. Naka, Y. Kai, S. Harada, N. Kasai, *J. Am. Chem. Soc.* **1983**, *105*, 7171–7172.
[9] K. Yamamoto, *Pure Appl. Chem.* **1993**, *65*, 157–163.
[10] K. Kawasumi, Q. Zhang, Y. Segawa, L. T. Scott, K. Itami, *Nat. Chem.* **2013**, *5*, 739–744.
[11] J. Luo, X. Xu, R. Mao, Q. Miao, *J. Am. Chem. Soc.* **2012**, *134*, 13796–13803.
[12] K. Y. Cheung, X. Xu, Q. Miao, *J. Am. Chem. Soc.* **2015**, *137*, 3910–3914.
[13] C.-N. Feng, M.-Y. Kuo, Y.-T. Wu, *Angew. Chem. Int. Ed.* **2013**, *52*, 7791–7794; *Angew. Chem.* **2013**, *125*, 7945–7948.
[14] Y. Sakamoto, T. Suzuki, *J. Am. Chem. Soc.* **2013**, *135*, 14074–14077.
[15] R. W. Miller, A. K. Duncan, S. T. Schneebeli, D. L. Gray, A. C. Whalley, *Chem. Eur. J.* **2014**, *20*, 3705–3711.
[16] F. Diederich, H. A. Staab, *Angew. Chem. Int. Ed. Engl.* **1978**, *17*, 372–374; *Angew. Chem.* **1978**, *90*, 383–385.
[17] H. Miyoshi, S. Nobusue, A. Shimizu, Y. Tobe, *Chem. Soc. Rev.* **2015**, *44*, 6560–6577.
[18] A. W. Robertson, G.-D. Lee, K. He, C. Gong, Q. Chen, E. Yoon, A. I. Kirkland, J. H. Warner, *ACS Nano* **2015**, *9*, 11599–11607.
[19] J. Bai, X. Zhong, S. Jiang, Y. Huang, X. Duan, *Nat. Nanotechnol.* **2010**, *5*, 190–194.
[20] S. Blankenburg, M. Bieri, R. Fasel, K. Müllen, C. A. Pignedoli, D. Passerone, *Small* **2010**, *6*, 2266–2271.
[21] D. Myśliwiec, M. Stępień, *Angew. Chem. Int. Ed.* **2013**, *52*, 1713–1717; *Angew. Chem.* **2013**, *125*, 1757–1761.
[22] M. A. Majewski, T. Lis, J. Cybińska, M. Stępień, *Chem. Commun.* **2015**, *51*, 15094–15097.
[23] B. Kumar, R. L. Viboh, M. C. Bonifacio, W. B. Thompson, J. C. Buttrick, B. C. Westlake, M.-S. Kim, R. W. Zoellner, S. A. Varganov, P. Mörschel, et al., *Angew. Chem. Int. Ed.* **2012**, *51*, 12795–12800; *Angew. Chem.* **2012**, *124*, 12967–12972.
[24] U. Beser, M. Kastler, A. Maghsoumi, M. Wagner, C. Castiglioni, M. Tommasini, A. Narita, X. Feng, K. Müllen, *J. Am. Chem. Soc.* **2016**, *138*, 4322–4325.
[25] M. Kondratowicz, D. Myśliwiec, T. Lis, M. Stępień, *Chem. Eur. J.* **2014**, *20*, 14981–14985.
[26] D. Myśliwiec, T. Lis, J. Gregoliński, M. Stępień, *J. Org. Chem.* **2015**, *80*, 6300–6312.
[27] D. Myśliwiec, B. Donnio, P. J. Chmielewski, B. Heinrich, M. Stępień, *J. Am. Chem. Soc.* **2012**, *134*, 4822–4833.
[28] B. Valeur, M. N. Berberan-Santos, *Molecular Fluorescence: Principles and Applications*, Wiley, Hoboken, **2013**.
[29] S. S. Zade, N. Zamoshchik, M. Bendikov, *Acc. Chem. Res.* **2011**, *44*, 14–24.
[30] R. E. Haddad, S. Gazeau, J. Pécaut, J.-C. Marchon, C. J. Medforth, J. A. Shelnutt, *J. Am. Chem. Soc.* **2003**, *125*, 1253–1268.
[31] A. H. Flood, *Beilstein J. Org. Chem.* **2016**, *12*, 611–627.
[32] W. B. Farnham, D. C. Roe, D. A. Dixon, J. C. Calabrese, R. L. Harlow, *J. Am. Chem. Soc.* **1990**, *112*, 7707–7718.
[33] S. S. Zhu, H. Staats, K. Brandhorst, J. Grunenberg, F. Gruppi, E. Dalcanale, A. Lützen, K. Rissanen, C. A. Schalley, *Angew. Chem. Int. Ed.* **2008**, *47*, 788–792; *Angew. Chem.* **2008**, *120*, 800–804.
[34] Y. Li, A. H. Flood, *Angew. Chem. Int. Ed.* **2008**, *47*, 2649–2652; *Angew. Chem.* **2008**, *120*, 2689–2692.
[35] S. Lee, C.-H. Chen, A. H. Flood, *Nat. Chem.* **2013**, *5*, 704–710.
[36] Y. Hua, R. O. Ramabhadran, E. O. Uduehi, J. A. Karty, K. Raghavachari, A. H. Flood, *Chem. Eur. J.* **2011**, *17*, 312–321.
[37] S. S. Pochapsky, H. Mo, T. C. Pochapsky, *J. Chem. Soc. Chem. Commun.* **1995**, 2513–2514.

Received: August 27, 2016
Published online: October 6, 2016

